Formation of ozone by solid state reactions

Journal:	*Physical Chemistry Chemical Physics*
Manuscript ID	CP-ART-05-2018-003020.R1
Article Type:	Paper
Date Submitted by the Author:	14-Jun-2018

Complete List of Authors:	Krim, Lahouari; UPMC Faculte de Chimie, Chimie Jonusas, Mindaugas; Sorbonne Université, CNRS, MONARIS, UMR 8233 Lemaire, Jean-Louis; bInstitut des Sciences Moléculaires d'Orsay (ISMO), CNRS - Université Paris-Sud Vidali, Gianfranco; Syracuse University, Department of Physics

SCHOLARONE™
Manuscripts

PCCP

ROYAL SOCIETY OF CHEMISTRY

ARTICLE TYPE

Cite this: DOI: 10.1039/xxxxxxxxxx

Formation of ozone by solid state reactions†

Lahouari Krim,*[a] Mindaguas Jonusas,[a] Jean Louis Lemaire,[a,b] and Gianfranco Vidali[a,‡]

Received Date
Accepted Date

DOI: 10.1039/xxxxxxxxxx

www.rsc.org/journalname

We studied the isotopic composition of ozone formed at low (3-10 K) temperature via O+O_2 solid state reactions using a partially dissociated $^{16}O/^{16}O_2$:$^{18}O/^{18}O_2$=1:1 mixture. The ozone ice has an isotopic abundance that differs from a statistical one and from gas phase studies. Ozone formation is influenced by the competition of production of O_2(O+O or O+O_3) vs. O_3 (O+O_2) and by the energy released in the O+O reaction. The exothermicity of the O+O reaction helps to overcome the barrier of the O+O_2 reaction. Heating the ozone ice past 50K brings about a transformation from amorphous to crystalline ice. Formation of ozone on water ice yields a blue shift of IR bands, and the yield of formed O_3 increases up to sample temperature of 100K. When $^{18}O/^{18}O_2$ is deposited on $H_2{}^{16}O$ ice, formation of $^{18}O^{18}O^{16}O$ is detected. We propose that the exothermicity of the reaction $^{18}O+^{18}O$ drives water dissociation ($^{16}O+H_2$) followed by ozone formation ($^{16}O+^{18}O_2 \rightarrow {}^{16}O^{18}O^{18}O$).

1 Introduction

Understanding the path to ozone formation and its isotopic signature is important in studies of icy solar system objects, since it can yield clues on the chemical origin and evolution of the Solar System, as well as in atmospheric physics[1]. In the gas-phase, ozone formation is understood to proceed according to the Chapman reaction:

$$O+O_2 + M \rightarrow O_3 + M$$

where M is a third body necessary to stabilize the products of reaction. Numerous studies have been done to probe this reaction, both because of the unusual isotopic ratio of the products and because of the complicated paths to ozone formation.

Two main unusual isotopic signatures are seen: a large enrichment of heavier isotopes with respect to what is expected; and a mass independent fractionation (for a review, see[1–3]). There is some uncertainty on the mechanisms of ozone formation that would yield such unusual isotopic composition but there is converging experimental evidence that it depends on pressure and temperature of oxygen in the gas-phase[4,5]. In the solid state, there have been fewer studies. Ozone formation in or on ice is important in space physics. For example, ozone has been detected on Ganymede[6] and on Saturn's satellites Rhea and Dione[7]. More in general, the isotopic ratios of oxygen in meteorites and in solar system ices is actively studied because it can be reveal pathways in the formation of the solar system[8].

The generation of ozone in the solid state is typically obtained using charged particles or UV light[9–11]. Schriver-Mazzuoli et al.[9] studied the vibrational spectrum of UV-generated O_3 in O_2 (pure and isotope mixed) or Ar matrices using the asymmetrical stretching ν_3 band and the bending ν_2 band. Bennett and Kaiser[12] and Sivaraman et al.[13] irradiated an ice of $^{16}O_2$ with 5 keV electrons to simulate the effect of bombardment of the solar wind on icy solar system bodies. The bombardment with electrons which created superthermal oxygen atoms which reacted with oxygen molecules to form ozone; ozone was also produced during a warm-up phase when thermalized oxygen atoms diffused and interacted with oxygen molecules. Ozone molecules were so obtained have the bent C_{2v} symmetry, while the cyclic D_{3h} ozone was not observed. Furthermore, spectroscopic evidence of a van der Waals complex of O_3 with O was obtained. In a subsequent investigation of electron induced fractionation in a mixture of $^{16}O_2$ and $^{18}O_2$ ices, Sivaraman et al.[14] found significant enrichment in ^{18}O bearing ozone, where $^{54}O_3$ was found to be six times more abundant than the lightest isotopologue $^{48}O_3$. Janssen[15], in gas phase studies found that there is no preference of asymmetric vs/ symmetric heavy ozone ($^{16}O^{16}O^{18}O/^{16}O^{18}O^{16}O$) beyond the statistical ratio.

Hydrogenation of solid state ozone is one of the routes to form water in the interstellar medium ($H+O_3 \rightarrow OH+O_2$; water is then formed through hydrogenation of OH or via $OH+OH \rightarrow H_2O_2$ and $H_2O_2+H \rightarrow H_2O+OH$. Jing et al.[16,17] studied the formation of ozone on an amorphous silicate as a stand-in for a dust grain in

[a] Sorbonne Université, CNRS, MONARIS, UMR 8233, F-75005, 4 place Jussieu, Paris,F-75005 France. E-mail: lahouari.krim@upmc.fr
[b] Institut des Sciences Moléculaires d'Orsay (ISMO), CNRS - Université Paris-Sud (UMR 8214), 91405 Orsay, France. E-mail: jean-louis.lemaire@u-psud.fr
‡ Permanent Address, Syracuse University, 201 Physics Bldg., Syracuse, NY 13244 , USA. E-mail: gvidali@syr.edu

the interstellar medium, using partially dissociated $^{16}O_2$ and $^{18}O_2$ beams converging on a silicate sample at 20K. No anomalous enrichment of heavy O_3 isotopologue was observed.

Here we present a study of ozone formation from a beam of a mixture of partially dissociated $^{16}O_2$ and $^{18}O_2$ deposited at 3 and 10 K on an inert substrate and at 3 K on water surface without any interaction with UV or charged particles.

2 Experimental

The experimental setup used in the present study has already been described previously[18], thus only important features are mentioned hereafter. The experiments are performed in a high vacuum chamber at 10^{-10} mbar. Solid samples are prepared by condensing gaseous mixtures of O/O_2 on the surface of a highly polished, Rh-plated copper mirror maintained at low temperature. O-atoms are formed by passing pure molecular oxygen ($^{16}O_2$ 99.9995% - Air Liquide and $^{18}O_2$ 99.0% - Isotec) through a microwave-driven radical atomic source (SPECS,PCS-ECR). Knowing the volume of the gas injection cell, the amount of O_2 injected during the deposition, at a rate of 1.6 μmol/min, is evaluated from the decrease of the O_2 pressure in the cell, measured with a digital Pirani gauge. The flux of O atoms is estimated to be about 10^{16} atoms cm^{-2} s^{-1} from the amount of molecular oxygen injected during the sample deposition, while the O_2-dissociation yield is measured to be $\sim$ 30% using a Quadrupole Mass Spectrometer (QMS - Hidden Analytical, a gas analyser with triple filter and pulse ion counting detection). The gas leaving the ECR plasma chamber is a combination of both atomic and molecular oxygen. We have investigated the solid state ozone formation by depositing O/O_2 mixture during 30 min at different temperatures ranged between 3 and 40 K. The resulting solid samples are analyzed by recording infrared spectra in the transmission-reflection mode between 5000 and 500 cm^{-1} using a Bruker Vertex 80v Fourier Infrared (FTIR) spectrometer with a KBr/Ge beam splitter and liquid N_2-cooled narrow band HgCdTe photoconductor. The angle of the IR beam is 8° with respect to the normal of the deposition mirror. A resolution of 0.5 cm^{-1} is used and 300 scans are recorded for each spectrum. The thickness e of the oxygen ice can be written as:

$$e = \frac{n_{O_2}}{\rho_{O_2}}$$

where n_{O2} and O_2 are the column density and the density of O_2 , respectively. According to Fulvio et al.[19] frozen O_2 at 20 K has a density ρ= 1.22 g cm^3. The n_{O2} column density[20] can be estimated from the integrated peak area of O_2 vibration at 1550 cm^{-1} and the strength of the infrared forbidden fundamental of O_2 (5 10^{-21} cm molecule^{-1}). In our experiments the thickness of the sample is around 3.5 μm. The solid samples have been heated progressively to different temperatures and monitored using IR and mass spectrometry. At each temperature step, during the heating process, the gas and solid phases are analyzed simultaneously by means of QM and IR spectrometers, respectively. O/O_2 depositions have been carried out both on the bare surface of the mirror and on the water ice covered surface to study the influence of water ice on O_3 formation. We investigate three specific astrophysically relevant points:

1. The influence of the temperature on the formation and structure of solid O_3 on an inert surface;

2. The O_3 isotopic distribution from solid to gas phase;

3. The influence of water ice covered surface on the formation and isotopic distribution of O_3.

3 Results

3.1 O/O_2 depositions on bare surfaces: the influence of the temperature on the formation and structure of solid O_3

Figure 1 shows the results of O/O_2 depositions at 3 and 10 K on the bare surface of the mirror. The IR spectra of the solid samples are dominated by the fundamental vibrational modes of O_2 at 1550.3 cm^{-1} and O_3 at 1034.4, 1103.2 and 701.5 cm^{-1}.

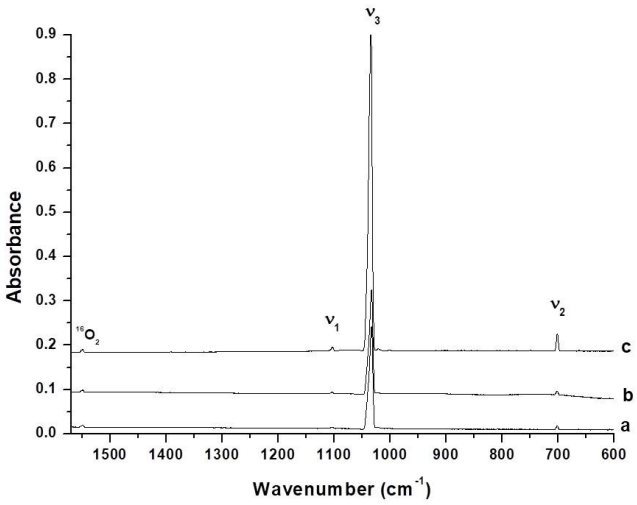

Fig. 1 a) Deposition of $^{16}O/^{16}O_2$ mixture at 3 K on the bare surface of the mirror. b) Sample heating from 3 to 10 K. c) Deposition of $^{16}O/^{16}O_2$ mixture at 10 K. ν_1, ν_2 and ν_3 are the vibrational modes of $^{16}O_3$.

Reactions occurring in the solid phase depend highly on the mobility of the reactants and on the sample deposition temperature. We observe the following:

- The amount of O_3 formed with a O/O_2 mixture deposited at 10 K is much larger than the one when the deposition is at 3 K, see Figures 1a and 1c.

- All O_3 formation following deposition of O/O_2 at 3 K occurs during the deposition itself. After deposition, the ice was kept for three hours and no change in the ν_3 IR band was observed, indicating that there is no significant mobility of oxygen atoms or molecules at 3 K.

- Increasing the sample temperature from 3 to 10 K yields a small ($<$ 10%) increase in O_3, see Figure 1b, due to the increased mobility of Oxygen atoms can react with O or O_3 to make O_2; however, a larger amount of O_3 is obtained by depositing O/O_2 at 10 K, see Figure 1c.

This journal is © The Royal Society of Chemistry [year]

- Heating the sample, whether produced by O/O_2 deposition at 3 or 10 K, to temperatures higher than 10 K yields a decrease of the O_3 signal. Figure 2 illustrates the evolution of the O_3 absorption bands between 10 and 50 K, where in addition to the O_3 signal decrease, the shapes of the ozone absorption bands change considerably. Figure 3 shows the behavior of the O_2 absorption band which disappears completely at 35 K.

These observations indicate that the O_3 formation occurs in solid phase through surface mobility of the reactants rather than in gas phase. If ozone formation had taken place in gaseous phase before being deposited, we would have detected the same amount of O_3 at 3 and 10 K. It should also be noted that no trace of O_3 has been detected in our mass spectra recorded during deposition, proving that the ozone formation actually takes place on the surface of the sample.

Oxygen atoms can react with O, O_2, and O_3 through the following reactions:

$O + O \rightarrow O_2$ (a)

$O + O_3 \rightarrow 2\,O_2$ $\quad k = 1.8x10^{-11}\ \exp(-2300/T)\ cm^3s^{-1}$ (b)

$O + O_2 \rightarrow O_3$ $\quad k = 6.4x10^{-35}\ \exp(-663/T)\ cm^3s^{-1}$ (c)

where the k values are for gas-phase reactions[21].

From a kinetics point of view, the O-O recombination Reaction (a) is much faster than Reaction (b) which, in turn, is less efficient than Reaction (c). Additionally, the low amount of O and O_3 trapped in the O_2-solid sample would suggest that the Reactions (a) and (b) would be less probable than Reaction (c) which involves O atoms and O_2 molecules in the solid sample. We have observed that, by heating the sample from 3 to 10 K, Reaction (a) is the most favorable and is actually in competition with Reaction (c). Reaction (a) is barrierless, but it needs O-atoms to be mobile in order to take place. In contrast, Reaction (c) has an energy barrier and cannot take place in solid phase at 3 K.

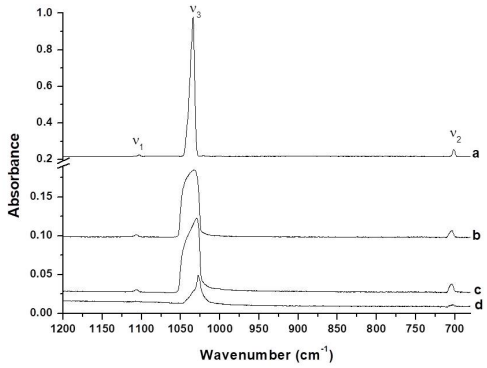

Fig. 2 O_3 spectral region. a) Deposition of $^{16}O/^{16}O_2$ mixture at 10 K. Successive sample heating to b) 35 K, c) 45 K, d) 50 K.

From the spectra of Figure 2, we notice that the large decrease of O_3 signal between 10 and 35 K is due only to the evaporation of O_2 from the ice, as shown in Figure 3. The IR spectra recoded between 35 and 50K (see Figure 2) show that the absorption bands of O_3 ice are temperature dependent, indicating a thermal re-organization of the O_3 ice structure.

Figures 4 and 5 show the evolution of ν_1, ν_2, ν_3, and $\nu_1+\nu_3$ absorption bands of O_3 ice for sequential sample heating between 35 and 50 K. This spectral evolution (spectral shifts and shape changes of the O_3 absorption bands) may directly be linked to transformations of the ozone ice morphology. Chaabouni et al.[22] have already reported that the ν_3 band is red shifted from 1037 to 1027 cm^{-1} for the ozone ice transformation from amorphous to crystalline phase. Similar spectral shifts as the ones of ν_1, ν_2, and ν_3 bands have also been noticed for the $\nu_1+\nu_3$ absorption band as shown in Figure 4. However the ν_2, ν_1, and $\nu_3+\nu_1$ absorption bands show behaviors different from that observed for ν_3 band.

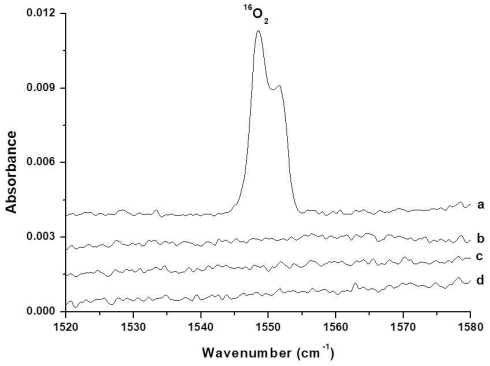

Fig. 3 O_2 spectral region. a) Deposition of $^{16}O/^{16}O_2$ mixture at 10K. Successive sample heating at b) 35 K, c) 45 K, and d) 50 K.

The ν_3 band located at 1037 cm^{-1} shifts to 1030 and 1027 cm^{-1} at 45K and 50K, respectively. Additionally, the ν_3 band is wide ($\sim$ 24 cm^{-1}) at temperatures lower than 45K and becomes narrow at 50K ($\sim$ 8 cm^{-1}), which is probably due to crystallization of O_3 ice. Similar behavior has been observed in O_3 ice obtained by direct deposition of O_3[23,24]. However, in our O/O_2 deposition at 3 K, the FWHM is narrower ($\sim$ 8 cm^{-1}) than at higher temperature and than the one in[23] ($\sim$ 16 cm^{-1}) because in our case O_3 is trapped in the O_2 crystal. When heated at 35 and 45 K, our FWHM are comparable to the ones of Ovchinnikov and Wight[23] and Chaabouni et al.[24]. During sample heating, the behavior of ν_1 and ν_2 bands is different from that of the ν_3 band. The spectral positions of ν_1 and ν_2 bands remain unchanged between 35 and 45 K, while, at 50 K, the ν_2 band is red shifted by 2 cm^{-1} (from 704 to 702 cm^{-1}), and ν_1 is blue shifted by 2 cm^{-1} (from 1106 to 1108 cm^{-1}). The ν_3 + ν_1 combination band is also shifted but its spectral shift is not consistent with the combination of the shifts measured for ν_3 and ν_1 absorption bands. In fact, during the sample heating from 35 to 50 K, ν_1 and ν_3 shift by -10 and +2 cm^{-1}, respectively. The ν_3 + ν_1 combination band position should shift by about -8 cm^{-1}; instead, we measure a shift of only -2 cm^{-1}. This could be due to differences in shapes of the ν_1 and ν_3 + ν_1 absorption bands (which are symmetric) vs. the ν_3 band (asymmetric). Table 1 lists the ν_1 ,ν_2 , ν_3 , and ν_3 + ν_1 absorption band positions (cm^{-1}) during the heating of O_3 ice.

From these results we notice that the morphology of O_3 ice formed in the O/O_2 deposition may be controlled by thermal processing between 10 and 50 K. At 10 K, the ozone is trapped in the

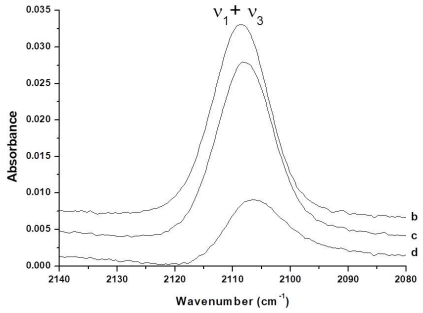

Fig. 4 Variation of the spectral positions of the $\nu_1 + \nu_3$ combination mode during successive sample heating at b) 35 K, c) 45 K, d) 50 K.

Table 1 ν_1 ,ν_2 , ν_3 , and $\nu_3 + \nu_1$ absorption band positions (in cm^{-1}) during the heating of O_3 ice.

T(K)	35	45	50
ν_1	1106	1106	1108
ν_2	704	704	702
ν_3	1037	1030	1027
$\nu_3 + \nu_1$	2109	2108	2107

oxygen matrix, while at 35 K all the O_2 molecules desorb, and the resulting O_3 ice has an amorphous structure. Between 35 and 45 K both amorphous and crystalline structures co-exist, while at 50 K only the crystalline phase of O_3 ice is favored. These successive phase transformations could be probed by measuring the variation of the spectral positions of the fundamental and combination vibrational modes of O_3 during heating as shown in Figures 3 and 4 and in Table 1. However, the most intense ν_3 absorption band of O_3 seems to be the privileged indicator for the O_3 ice structure vs. temperature shifts, as it has different shapes and different spectral positions during sample heating. The $\nu_1 + \nu_3$ combination band is also intense but it retains almost the same shape whatever the temperature of O_3 ice is, and it shifts by only 2 cm^{-1} for the O_3 amorphous-crystalline phase transformation. Such phase transformation has also been investigated by forming O_3 ice through O/O_2 deposition at temperatures higher than 30 K to avoid the condensation of O_2 molecules in order to have a pure ozone ice. Figure 5 compares the ν_3 band for O/O_2 deposition at 10, 30 and 40 K.

For O/O_2 deposition at 10 K, the narrow IR absorption signals corresponds to O_3 trapped in solid O_2. Formation of amorphous O_3 ice at 30 K is characterized by a broad symmetric shape of the ν_3 band, while O_3 ice formed at 40 K has an asymmetric narrower ν_3 band. We interpret this as the co-existence of an amorphous and crystalline phase, based on the following experiment. By depositing O/O_2 at 40 K, amorphous O_3 is formed, as evidenced from the broad and symmetric ν_3 band. By heating to 50 K, crystalline O_3 is formed (narrow ν_3 band). The ν_3 band is measurable till 60 K and disappears completely at 65 K (see Figure 6). We note that the ν_3 band at 50 K has a blue tale, while there is hardly one in Chaabouni et al. [22], perhaps because of kinetic effects.

Next we show that the formation of O_3 through O/O_2 deposition is efficient for deposition temperatures ranged between 3

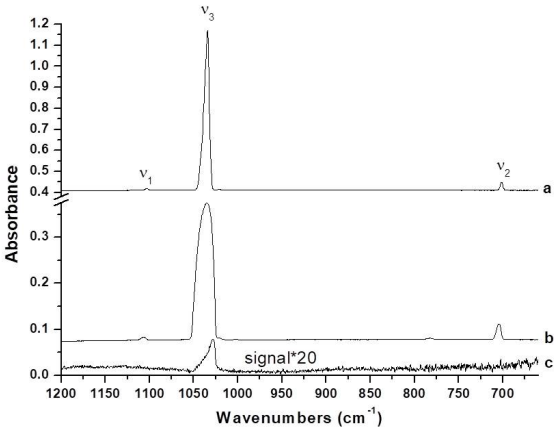

Fig. 5 Evolution of absorption bands of O_3 formed through $^{16}O/^{16}O_2$ deposition at: a) 10 K, b) 30 K, c) 40 K.

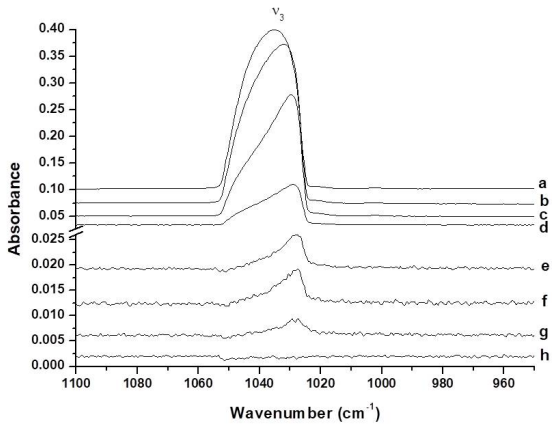

Fig. 6 Evolution on ν_3 absorption band of O_3 ice formed at 30 K. a) $^{16}O/^{16}O_2$ deposition at 30 K. Successive sample heating to: b) 35 K, c) 40 K, d) 45 K, e) 50 K, f) 55 K, g) 60 K, h) 65 K.

and 40 K. Amorphous O_3 ice is formed in deposition at 30 K, and a mixture of amorphous and crystalline is found for deposition at 40 K. In order to better monitor the O + O_2 solid state reaction, we have investigated the O_3 formation on the surface of water ice. Since water ice traps both O and O_2 species which are well separated from each other, the O-O_2 interaction can be probed by controlling the mobility of the two reactants O and O_2 during H_2O-ice heating. We investigated the deposition of the isotopic mixture $^{18}O/^{18}O_2$ on the surface of $H_2^{16}O$-ice at 3 K and measured the amount of $^{18}O^{18}O^{18}O$, $^{18}O^{16}O^{18}O$ and $^{16}O^{18}O^{18}O$ formed during the sample heating. The two reaction products $^{18}O^{16}O^{18}O$ and $^{16}O^{18}O^{18}O$ containing ^{16}O - where ^{16}O comes from $H_2{}^{16}O$ ice, are good markers for the role played by water ice in the O_3 intramolecular isotope distribution. Consequently, two additional experiments have been carried out:

- Deposition of $^{16}O/^{16}O_2$ - $^{18}O/^{18}O_2$ (1:1) mixture at 3 K on an inert surface, in order to characterize the isotopic distri-

This journal is © The Royal Society of Chemistry [year]

bution of O_3 in solid phase by measuring the amounts of ozone isotopomers during the reaction at different temperatures.

- Deposition of pure mixture $^{18}O/^{18}O_2$ on $H_2^{16}O$-ice at 3 K in order to characterize the influence of water molecules on the formation and isotopic distribution of O_3 by probing the production of $^{18}O_3$ and of all isotopomers containing at least one ^{16}O-atom derived from water ice.

3.2 Deposition of $^{16}O/^{16}O_2$ - $^{18}O/^{18}O_2$ (1 : 1) mixture on bare surfaces: O_3 isotopic distribution from solid to gas phase

Sivaraman et al.[14] studied the formation of six ozone isotopomers in electron-irradiation of solid oxygen deposited at 11 K and made of $^{16}O_2$-$^{18}O_2$ (1:1). They formed all the isotopic species $^{16}O^{16}O^{16}O$, $^{18}O^{18}O^{18}O$, $^{16}O^{18}O^{18}O$, $^{18}O^{18}O^{16}O$, $^{16}O^{18}O^{16}O$, and $^{18}O^{16}O^{18}O$. They showed that the heavy $^{18}O^{18}O^{18}O$ species was formed with a factor of about six more efficiently than $^{16}O^{16}O^{16}O$. On the other hand, they showed that while there was no isotope effect in the production of $^{16}O^{18}O^{16}O$ versus $^{18}O^{16}O^{18}O$, the heavier asymmetric species $^{18}O^{18}O^{16}O$ was formed with abundance of about a factor of three higher than the lighter asymmetric $^{16}O^{16}O^{18}O$.

In order to characterize, under our experimental conditions, the isotopic distribution of O_3 formed in solid phase, we deposited at 3 K a discharged mixture $^{16}O_2$-$^{18}O_2$ (1:1). Figure 7 shows a comparison between $^{16}O/^{16}O_2$ and $^{16}O/^{16}O_2$ - $^{18}O/^{18}O_2$ depositions in the ν_1 and ν_3 spectral region. We will use hereafter the notation xyz to qualify the ozone isotope $^{1x}O^{1y}O^{1z}O$, where x, y and z are either 6 or 8.

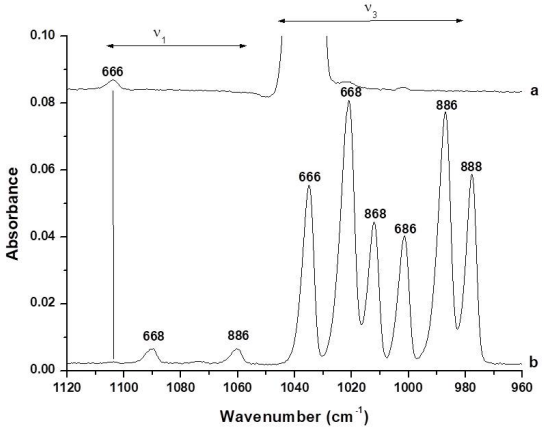

Fig. 7 Comparison of deposition on a 3 K surface of: a) pure $^{16}O_2$ subjected to a discharge. b) $^{16}O_2$ -$^{18}O_2$ (1:1) mixture subjected to a discharge. The 16/18 ozone isotopomers $^{16}O^{16}O^{16}O$, $^{16}O^{16}O^{18}O$, $^{18}O^{16}O^{18}O$... are labeled as 666, 668, 868...

Figure 7 shows that the O_3 isotopic distribution in the ν_3 region is statistical and different from that of Sivaraman et al.[14].

Figure 8 shows that when heating the sample from 3 to 10 K there is only a 10% increase of the O_3 signal. However, all the O_3 peaks increase similarly and there is no evidence that the heaviest $^{18}O^{18}O^{18}O$ is favored over lighter species. Figure

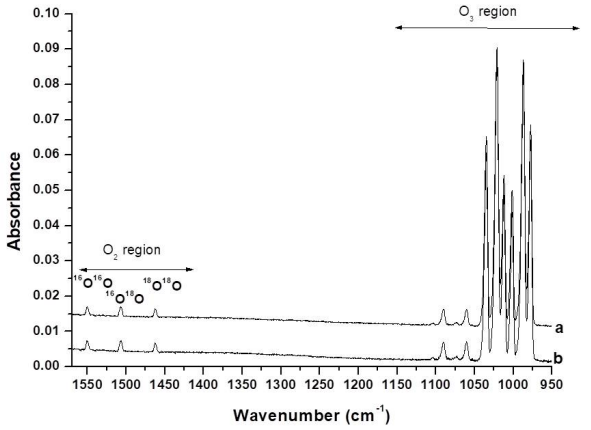

Fig. 8 Deposition on a 3 K surface of a $^{16}O_2$ -$^{18}O_2$ (1 : 1) mixture with discharge on. a) After sample deposition at 3 K. b) After sample heating from 3 to 10 K

9 shows the results when heating the sample formed at 3K at temperatures ranged between 10 and 40 K. The heating of the sample at temperatures higher than 10 K leads to the desorption of O_2 molecules with a consequent decrease of all the IR signals. Above 30 K, O_2 signatures disappear showing that all O_2 molecules are desorbed. The recorded spectra of the resulting O_3 ice show the same statistical isotopic distribution resulting from $^{16}O/^{16}O_2$ + $^{18}O/^{18}O_2$ recombinations where the asymmetric isotopes $^{16}O^{16}O^{18}O$ and $^{18}O^{18}O^{16}O$ have the highest IR intensities, whatever the temperature of the sample is.

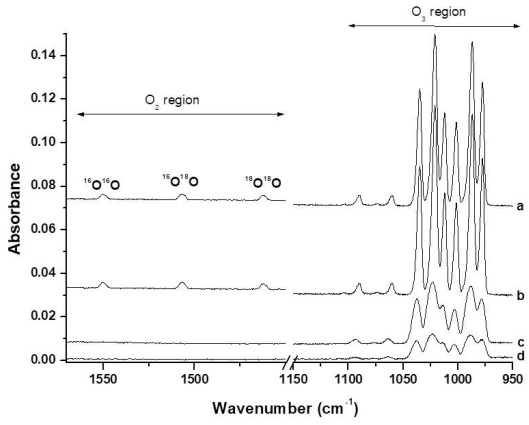

Fig. 9 Deposition on a 3 K surface of a $^{16}O_2$ -$^{18}O_2$ (1 : 1) mixture with discharge on. a) After sample deposition at 3 K. After sample heating at: b) 10 K, c) 30 K, and d) 40 K.

We have calculated the isotopic distribution of O_3 for the two extreme temperatures, 3 and 40 K. At 3 K, O_3 is trapped in solid O_2, while at 40 K O_3 molecules form an amorphous ozone ice. Figure 10 and Table 2 show the O_3 isotopic abundances in the

solid phase estimated from the integrated areas of the absorption peaks of each isotopic species.

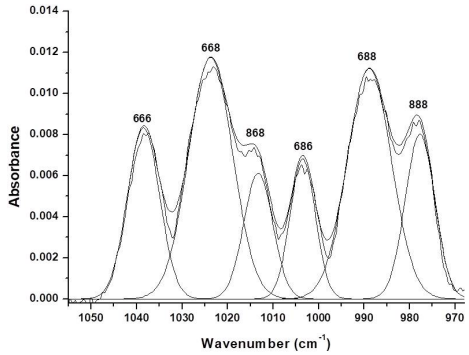

Fig. 10 Gaussian fit of the ν_3 peaks for a sample heated to 40 K. The 16/18 ozone isotopomers are labeled as in Figure 7

Table 2 O_3 isotopic distribution calculated from O_3 peak area integration (S) at 3 and 40 K.

isotope	a	b	c	d	e	f	T(K)	
S(cm^{-1})	0.30	0.50	0.18	0.18	0.50	0.30	3	
S(cm^{-1})	0.07	0.14	0.05	0.05	0.14	0.07	40	
Mass	M48	M50		M52		M54		

a=$^{16}O^{16}O^{16}O$
b=$^{16}O^{16}O^{18}O$
c=$^{16}O^{18}O^{16}O$
d=$^{18}O^{16}O^{18}O$
e=$^{16}O^{18}O^{18}O$
f=$^{18}O^{18}O^{18}O$

From figure 10 and table 2, we see that the pairs of isotopomers, the asymmetric $^{16}O^{16}O^{18}O$ and $^{18}O^{18}O^{16}O$, the symmetric $^{18}O^{16}O^{18}O$ and $^{18}O^{16}O^{18}O$, and the totally symmetric $^{16}O^{16}O^{16}O$ and $^{18}O^{18}O^{18}O$ are formed with the same abundances, both in the O_3 ice at 40 K and also for O_3 isolated in solid O_2 at 3 K. However, we notice that the isotopic distributions of O_3 formed in solid phase are different from those reported in previous gas-phase studies where O_3 isotopomers produced by electric or microwave discharge of $^{16}O_2$ -$^{18}O_2$ (1:1) mixtures[15]. Janssen[15] showed that in O_3 formation in the gas-phase, the ratio of asymmetric $^{16}O^{16}O^{18}O$ vs symmetric $^{18}O^{16}O^{18}O$ is 2.13 at 360 K and decreases to 2.00 at 170K. Under our experimental conditions, the ratios [$^{16}O^{16}O^{18}O$] /[$^{16}O^{18}O^{16}O$] and [$^{16}O^{18}O^{18}O$] /[$^{18}O^{16}O^{18}O$] are equal to 2.8, which shows that the formation of asymmetric over symmetric ozone is amplified by 30% when O_3 formation occurs| in solid phase. As the O_3 isotopic distributions are similar in the solid phase both at 3 and 40K, we would think that the O_3 molecules keep the same isotopic distributions in the gas-phase during the thermal desorption of O_3 ice. Figure 11 shows the mass spectra recorded during sample desorption that takes place between 60 and 66 K. Table 3 compares O_3 isotopic abundances in solid (at 40 K) and gas phase during O_3 desorption. it shows that, relative to the totally symmetric $^{16}O_3$ or $^{18}O_3$ species, the abundance of the scrambled isotopomers of ozone is much higher in the solid phase than in the gas phase.

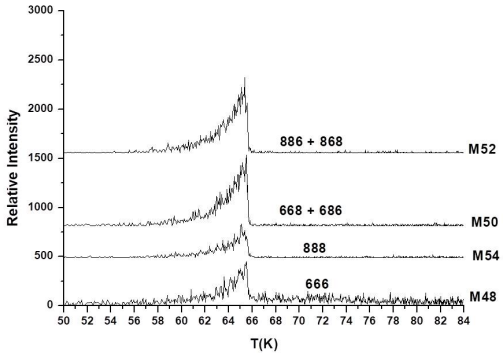

Fig. 11 Desorption of the six ozone isotopomers from O_3 ice. The 16/18 ozone isotopomers are labeled as in Figure 7.

Table 3 O_3 isotopic abundances in solid and gas phases (this work).

isotope	a	b	c	d	e	f
Mass	M48	M50		M52		M54
Solid phase	1	2.7		2.7		1
Gas phase	1	2.1		2.1		1

a=$^{16}O^{16}O^{16}O$
b=$^{16}O^{16}O^{18}O$
c=$^{16}O^{18}O^{16}O$
d=$^{18}O^{16}O^{18}O$
e=$^{16}O^{18}O^{18}O$
f=$^{18}O^{18}O^{18}O$

Form these results, we notice that the O_3 isotopic distribution depends not only on where the ozone formation reaction takes place but also on O_3 desorption processes from the solid to the gas phase.

3.3 Deposition of $^{18}O/^{18}O_2$ on $H_2^{16}O$-ice: the influence of water ice covered surface on the formation and isotopic distribution of O_3

Figure 12 shows the results of the co-deposition of $^{18}O/^{18}O_2$ on $H_2^{16}O$ ice at 3 K and the successive sample heating between 3 and 170 K. Due to the interaction with water ice, the ν_3 and $\nu_1 + \nu_3$ bands of $^{18}O_3$ are broad and blue shifted in comparison with the IR signals obtained with a deposition of $^{16}O_2$ - $^{18}O_2$ (1 : 1) mixture (discharge on) on a bare surface.

By taking as a reference the spectrum in Figure 12a recorded for the $^{16}O_2$ -$^{18}O_2$ (1 : 1) experiment that was carried out to characterize the O_3 isotopic distribution, we notice from the spectrum in Figure 12b, that for the deposition of $^{18}O/^{18}O_2$ (discharge on) on $H_2^{16}O$ ice at 3K, the main isotope formed is $^{18}O_3$ trapped in mixed $^{18}O_2$-$H_2^{16}O$ ice. Additionally small amounts of $^{18}O^{16}O^{18}O$ symmetric heavy and $^{16}O^{16}O^{18}O$ asymmetric light isotopomers are also formed. However, the $^{18}O_3$ bands observed in Figure 12b is broad and it may hide the signal due to the asymmetric heavy $^{16}O^{18}O^{18}O$.

This journal is © The Royal Society of Chemistry [year]

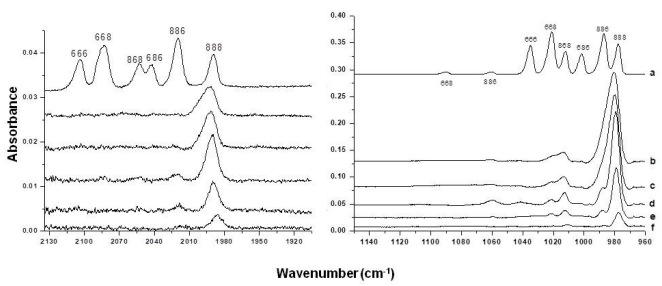

Fig. 12 $\nu_1 + \nu_3$ (left) and ν_3 (right) spectral regions. a) Deposition on a 3 K surface of a $^{16}O_2$ -$^{18}O_2$ (1 : 1) mixture with discharge on. b) Deposition of $^{18}O/^{18}O_2$ (discharge on) on $H_2^{16}O$ ice at 3 K. c) though f): heating of the sample formed at 3 K by depositing $^{18}O/^{18}O_2$ (discharge on) on $H_2^{16}O$ ice at: 50 K, 100 K, 150 K, and 170 K, respectively. The 16/18 ozone isotopomers are labeled as in Figure 7.

In order to control the formation of O_3 on water ice, we have gradually heated the solid sample formed at 3K. Spectra in Figures 12c-12f show the result of heating the sample. In contrast with the O/O_2 deposition on a bare surface at 3 K, the O_3 signal begins increasing not between 3 and 10 K, but only when the heating temperature reaches 50 K. At 100 K the O_3 amount reaches a maximum and the ν_3 band shows an isotopic structure where the signals due to $^{18}O^{18}O^{18}O$, $^{16}O^{18}O^{18}O$ and $^{18}O^{16}O^{18}O$ are clearly visible (spectrum in Figure 12d). At temperatures higher than 100 K, the O_3 molecules start to desorb and the signal disappears completely at 190 K. In the spectra recorded between 100 and 150 K, the IR signals of $^{16}O^{18}O^{18}O$ and $^{18}O^{16}O^{18}O$ have almost the same intensity. Consequently, both symmetric and asymmetric heavy ozone form efficiently on water ice and there is no preference for the formation of asymmetric over symmetric O_3, while with the deposition of a $^{16}O_2$ - $^{18}O_2$ (1 : 1) mixture on a bare surface, the abundance of $^{16}O^{18}O^{18}O$ is three times higher than that of $^{18}O^{16}O^{18}O$.

4 Discussion

We investigated the formation of O_3 in solid phase by depositing O/O_2 mixtures onto an inert substrate at 3 and 10 K and showed that the O_3 formation is strongly temperature dependent. Experiments carried out at 10 K show that the maximum amount of O_3 is reached during the sample deposition, and subsequent heating of the sample at temperatures higher than 10 K leads mainly to the decrease of the O_3 abundance. Similar experiments carried out at 3 K show that O_3 solid state formation can be monitored by heating the O/O_2 ice between 3 and 10 K. However, all the sample heatings at temperatures higher than 10 K lead only to the consumption of O_3, regardless of the deposition temperature. The formation of O_3 through a O/O_2 deposition on a water surface ice at 3 K shows that the O_3 solid state formation might be monitored in a large temperature range. The amount of O_3 increases when the sample is heated from 3 to 50 K, reaches its maximum at 100K and decreases at higher temperatures.

Many theoretical studies have shown that the formation of O_3 through the $O(^3P) + O_2(^3\Sigma_g^-)$ ground state reaction has an energy barrier between 5 and 28 kJ/mol[25], depending on the atomic basis size used. Such a barrier would explain the increase of O_3 in our solid samples during the heating between 3 and 10 K. The O_3 increase would then be induced by the energy released during the O + O recombination reaction which is more favorable at 10 than at 3 K. The energy released from O + O recombination that leads to the formation of ground state $O_2(^3\Sigma_g^-)$ is almost 5 eV[26] which may be absorbed by the O_2-matrix. However, the O + O recombination may also lead to the formation of long-lived metastable states of O_2 such as $O_2(^1\Sigma_g^+)$ or $O_2(^1\Sigma_u^-)$ with energies of 1.6 and 4.2 eV, respectively. These metastable species may be trapped in the O_2-matrix and react with $O(^3P)$ to form O_3.

Clyne et al.[27] have investigated the formation of $O_2(^1\Sigma_g^+)$ metastable through $O(^3P) + O(^3P)$ recombination by probing the emission - centered around 760 nm, in the transition $O_2(^1\Sigma_g^+) \rightarrow O_2(^3\Sigma_g^-)$. The existence in solid phase of electronic states with different spin multiplicity of O_2 has been investigated by Akimoto and Pitts[28] by studying the emission spectra of $O_2(^1\Delta_g) \rightarrow O_2(^3\Sigma_g^-)$ in pure solid oxygen at 4 K. Such studies would confirm that O_3 might be formed, under our experimental conditions, in two steps involving $O_2(^1\Sigma_g^+)$ as reaction intermediate. The energy gain (1.6 eV) can induce the reaction:

$$O(^3P) + O\ (^3P) \rightarrow O_2(^1\Sigma_g^+) \quad (1)$$
$$O_2(^1\Sigma_g^+) + O(^3P) \rightarrow O_3 \quad (2)$$

The same Clyne et al.[27] study has also shown that the metastable $O_2(^1\Sigma_g^+)$ and ground sate atomic oxygen $O(^3P)$ are closely tied. The $O(^3P) + O_3$ reaction is a source of the metastable $O_2(^1\Sigma_g^+)$, while $O_2(^1\Sigma_g^+) + O_3$ leads to the formation of $O(^3P)$.

$$O(^3P) + O_3 \rightarrow O_2(^1\Sigma_g^+) + O_2(^3\Sigma_g^-) \quad (3)$$
$$O_2(^1\Sigma_g^+) + O_3 \rightarrow O(^3P) + 2O_2(^3\Sigma_g^-) \quad (4)$$

Our O_3 solid state formation experiments carried out at 3 K on an inert substrate showed that the amount of O_3 increases only during the sample heating from 3 and 10 K. Any heating at temperatures higher than 10 K leads mainly to a decrease of the O_3 amount. This shows that reactions involving mainly atomic oxygen (Reactions (1) and (2)) are predominant in the 3-10 K temperature range, while Reactions (3) and (4), which involve much heavier species such as O_3 and O_2, are more favorable at temperatures higher than 10 K.

We also showed that, when similar experiments are carried out at 3 K on water ice surfaces, the O_3 formation is favored at temperatures between 50 and 100 K. At temperatures higher than 100 K, the amount of O_3 begins to decrease, probably due to the O_3 consumption through Reactions (3) and (4), in addition to O_3 desorption. However, our experimental results show that the formation of O_3 on water ice cannot be due to only Reactions (1)

and (2), which are induced just by the thermal mobility of oxygen atoms. In fact, the heating of the sample formed by deposition of $^{18}O/^{18}O_2$ on the $H_2{}^{16}O$ ice surface leads not only to $^{18}O_3$ formation which can be directly linked to Reactions (1) and (2), but also to the production, with almost the same concentrations, of mixed isotopic species such as $^{16}O^{18}O^{18}O$ and $^{18}O^{16}O^{18}O$. This would suggest that water molecules are really involved in O_3 formation. In fact, under our experimental conditions, the only source of ^{16}O in the production $^{16}O^{18}O^{18}O$ and $^{18}O^{16}O^{18}O$ species is from the dissociation of $H_2{}^{16}O$ molecules. As we mentioned earlier, the heating of the sample leads to the $^{18}O(^3P)$ + ^{18}O (^3P) recombination to form $^{18}O_2(^3\Sigma_g^-)$, $^{18}O_2(^1\Sigma_g^+)$ and $^{18}O_2(^1\Sigma_u^-)$, with a gain of energy between 1.6 and 5 eV. The energy released during the formation of ground state $^{18}O_2(^3\Sigma_g^-)$ is high enough to allow the dissociation of $H_2{}^{16}O$ to $^{16}O(^3P)$ + H_2 [29]. Consequently, the $^{16}O(^3P)$ from water ice produced during $^{18}O(^3P)$ + ^{18}O (^3P) recombination may react with the $O_2(^1\Sigma_g^+)$ metastable to form $^{16}O^{18}O^{18}O$ and $^{18}O^{16}O^{18}O$ in three steps as follows:

Step1: Dissociation of $H_2{}^{16}O$

$^{18}O(^3P) + {}^{18}O\ (^3P) + H_2{}^{16}O \rightarrow {}^{18}O_2(^3\Sigma_g^-) + H_2 + {}^{16}O(^3P)$ (5)

Step 2: Formation $O_2(^1\Sigma_g^+)$ metastable

$^{18}O(^3P) + {}^{18}O\ (^3P) + H_2{}^{16}O \rightarrow {}^{18}O_2(^1\Sigma_g^+) + H_2{}^{16}O$ (6)

$^{18}O(^3P) + {}^{16}O\ (^3P) + H_2{}^{16}O \rightarrow {}^{18}O^{16}O\ (^1\Sigma_g^+) + H_2{}^{16}O$ (7)

Step 3: Formation O_3

$^{18}O_2(^1\Sigma_g^+) + {}^{18}O(^3P) \rightarrow {}^{18}O_3$ (8)

$^{18}O_2(^1\Sigma_g^+) + {}^{16}O\ (^3P) \rightarrow {}^{18}O^{18}O^{16}O$ (9)

$^{18}O\ (^3P) + {}^{18}O^{16}O\ (^1\Sigma_g^+) \rightarrow {}^{18}O^{18}O^{16}O$ (10)

$^{18}O^{16}O\ (^1\Sigma_g^+) + {}^{18}O\ (^3P) \rightarrow {}^{18}O^{16}O^{18}O$ (11)

Under our experimental conditions where the $^{18}O/^{18}O_2$ mixture is deposited on $H_2{}^{16}O$ ice, in addition to the formation of main ozone isotope $^{18}O_3$ which may occur through Reactions (6) and (8), the formation of $^{16}O^{18}O^{18}O$ and $^{18}O^{16}O^{18}O$ mixed species depends strongly on the efficiency of Reaction (5). As the $^{16}O(^3P)$ is a secondary product during the formation of O_3 and derives from Reaction (5), we should take into consideration only reaction mechanisms involving one ^{16}O atom to from either $^{16}O^{18}O^{18}O$ or $^{18}O^{16}O^{18}O$. Then for a given amount of $^{16}O(^3P)$ formed during the heating of the sample, reactions leading to $^{16}O^{18}O^{18}O$ and $^{18}O^{16}O^{18}O$ occur with equal probability and both of them involve two ^{18}O-atoms and one ^{16}O-atom (Reactions (7) and (11) for $^{18}O^{16}O^{18}O$; Reactions (6) or (7) and (9) or (10) for $^{16}O^{18}O^{18}O$). These mechanisms are in good agreement with our observations, in which the IR signals of $^{16}O^{18}O^{18}O$ and $^{18}O^{16}O^{18}O$ have almost the same intensity during the sample heating. In order to bring further insight into the formation of symmetric and asymmetric ozone, we have investigated reactions where the reactants are 50% $^{18}O/^{18}O_2$ + 50% $^{16}O/^{16}O_2$ obtained from $^{16}O_2$ - $^{18}O_2$ (1 : 1) mixture subjected to a microwave discharge. We have shown experimentally that both heavy and light ozone form efficiently and the abundance of the asymmetric ozone is three times higher than of that of the symmetric one. Based on reactions 1 and 2, we can consider all the O and O_2 isotopic species involving into the formation of O_3 through $^{18}O/^{18}O_2$ + $^{16}O/^{16}O_2$ reaction, as follows:

Step 1: Formation $O_2(^1\Sigma_g^+)$ metastable

$^{16}O(^3P) + {}^{16}O\ (^3P) \rightarrow {}^{16}O^{16}O\ (^1\Sigma_g^+)$

$^{18}O(^3P) + {}^{16}O\ (^3P) \rightarrow {}^{18}O^{16}O\ (^1\Sigma_g^+)$

$^{18}O(^3P) + {}^{18}O\ (^3P) \rightarrow {}^{18}O^{18}O\ (^1\Sigma_g^+)$

Step 2: Formation O_3

$^{16}O^{16}O^{16}O$

$^{16}O^{16}O\ (^1\Sigma_g^+) + {}^{16}O(^3P) \rightarrow {}^{16}O^{16}O^{16}O$

$^{16}O^{16}O^{18}O$

$^{16}O^{16}O\ (^1\Sigma_g^+) + {}^{18}O(^3P) \rightarrow {}^{16}O^{16}O^{18}O$

$^{18}O^{16}O\ (^1\Sigma_g^+) + {}^{16}O(^3P) \rightarrow {}^{18}O^{16}O^{16}O$

$^{16}O^{18}O^{16}O$

$^{16}O(^3P) + {}^{18}O^{16}O\ (^1\Sigma_g^+) \rightarrow {}^{16}O^{18}O^{16}O$

$^{18}O^{16}O^{18}O$

$^{18}O^{16}O\ (^1\Sigma_g^+) + {}^{18}O(^3P) \rightarrow {}^{18}O^{16}O^{18}O$

$^{18}O^{18}O^{16}O$

$^{18}O(^3P) + {}^{18}O^{16}O\ (^1\Sigma_g^+) \rightarrow {}^{18}O^{18}O^{16}O$

$^{18}O^{18}O\ (^1\Sigma_g^+) + {}^{16}O(^3P) \rightarrow {}^{18}O^{18}O^{16}O$

$^{18}O^{18}O^{18}O$

$^{18}O^{18}O\ (^1\Sigma_g^+) + {}^{18}O(^3P) \rightarrow {}^{18}O^{18}O^{18}O$

We notice that the formation of asymmetric ozone such as $^{18}O^{18}O^{16}O$ or $^{16}O^{16}O^{18}O$ is twice more probable than the formation of symmetric ozone such as $^{18}O^{16}O^{18}O$ or $^{16}O^{18}O^{16}O$. This is a statistical isotopic distribution which is in good agreement with the gas phase O_3 formation. Janssen et al. [30] has already measured, ratios of asymmetric $^{16}O^{16}O^{18}O$ vs symmetric $^{16}O^{18}O^{16}O$ of 2.13 and 2.00 at 360 K and 170 K, respectively. From our measurements we notice that the isotopic distributions of O_3 formed in solid phase is different from those reported in gas phase and then from the statistical isotopic distribution of O_3. We have measured the $[^{16}O^{16}O^{18}O]$ /$[^{16}O^{18}O^{16}O]$ and $[^{16}O^{18}O^{18}O]$ /$[^{18}O^{16}O^{18}O]$ ratios equal to 2.8 showing that the formation of asymmetric over symmetric ozone is amplified by 30% when the O_3 formation occurs in $^{16}O/^{16}O_2$ + $^{18}O/^{18}O_2$ solid phase mixture rather than in the gas phase. Additionally, we did not observe any oxygen mass dependence in the O_3 solid state formation, as suggested by the gas phase study carried out by Janssen et al. [30]. That study underlines that the mass of the oxygen atom plays a huge role in the kinetic of the formation of isotopic ozone and that the heavy ozone can be formed more efficiently than the light one [30]. Janssen et al. [30] have shown that molecular oxygen attacked by lighter atoms tends to give the larger rates. Therefore, the reaction $^{16}O + {}^{18}O^{18}O \rightarrow {}^{16}O^{18}O^{18}O$ should be faster than $^{18}O + {}^{16}O^{16}O \rightarrow {}^{18}O^{16}O^{16}O$ and the amount of $^{16}O^{18}O^{18}O$

This journal is © The Royal Society of Chemistry [year]

formed through a fast channel should be higher than that of $^{18}O^{16}O^{16}O$. Instead, we measure that[$^{16}O^{18}O^{18}O$]/[$^{18}O^{16}O^{16}O$] is equal to 1.

5 Conclusions

We studied the formation of ozone in the solid state in order to obtain information on the mechanisms of formation and on the isotopic distribution. We investigated three points:

1. The influence of the temperature on the formation and structure of solid O_3. The formation of ozone is temperature dependent, with a marked increase from 3 to 10 K, likely due to the increase mobility of O that produces more O_2; the energy released helps overcome the barrier to the $O+O_2$ reaction. At 10 K, the formation of ozone occurs through Reactions (1) and (2). At temperatures higher than 10 K, ozone is destroyed, see Reactions (2) and (3). There is a transition from amorphous ozone ice to crystalline at 50 K.

2. The influence of water molecules on the formation and isotopic distribution of O_3. On a amorphous solid water substrate, the energy released in the O+O reaction dissociates water, and the freed ^{16}O atom can form O_3 via reactions with $^{18}O_2$. Differently from the formation of ozone on an inert substrate, the formation of O_3 on water ice increases from 50 to 100K.

3. The O_3 isotopic distribution from the solid to gas phases. On an inert substrate, starting with a $^{16}O/^{16}O_2$ - $^{18}O/^{18}O_2$ (1 : 1) mixture, O_3 is formed with isotopic distribution that shows no preference for heavier isotopes, differently from the result in[14] that used electron irradiation of O_2 ice, or from the gas phase results[30]; furthermore, asymmetric ozone $^{16}O^{18}O^{18}O$ is 2.8 more abundant than symmetric $^{18}O^{16}O^{18}O$. The ratio of asymmetric/symmetric ozone is 30% higher than measured in gas phase reactions, and higher than the statistical distribution (x2). Gas phase studies hint that ozone isotopic anomaly is due to strong isotopic dependence in the formation reactions[31]; the work presented here shows that also in the solid state there is an anomaly in the ratio of asymmetric/symmetric isotopologues, but the heavy isotopologues are not over-represented with respect to what is expected stochastically. Our results of ozone formation by atom addition differ from the isotopic fingerprint of ozone generated by the interaction of energetic radiation with solid O_2[14]. Such results should help in uncovering the origin of ozone in solar system bodies.

Acknowledgments

G.V. would like to acknowledge financial support from UPMC and NSF, Division of Astronomical Sciences Grant #1615897. This work was supported in part by the LabEx MiChem "French state funds managed by the ANR within the Investissements d'Avenir programme under reference ANR-11-IDEX-0004-02."

References

1 M. H. Thiemens, Proceedings of the National Academy of Science, 2013, **110**, 17631–17637.
2 R. Schinke, S. Y. Grebenshchikov, M. Ivanov and P. Fleurat-Lessard, Annual Review of Physical Chemistry, 2006, **57**, 625–661.
3 K. Mauersberger, D. Krankowsky and C. Janssen, Surface Science Reviews, 2003, **106**, 265–279.
4 Y. Q. Gao and R. A. Marcus, Journal of Chemical Physics, 2007, **127**, 244316–244316.
5 K. L. Feilberg, A. A. Wiegel and K. A. Boering, Chemical Physics Letters, 2013, **556**, 1–8.
6 K. S. Noll, R. E. Johnson, A. L. Lane, D. L. Domingue and H. A. Weaver, Science, 1996, **273**, 341–343.
7 K. S. Noll, T. L. Roush, D. P. Cruikshank, R. E. Johnson and Y. J. Pendleton, Nature, 1997, **388**, 45–47.
8 R. A. Marcus, J Chem Physics, 2004, **121**, 8201–8211.
9 L. Schriver-Mazzuoli, A. de Saxcé, C. Lugez, C. Camy-Peyret and A. Schriver, Journal of Chemical Physics, 1995, **102**, 690–701.
10 B. D. Teolis, M. J. Loeffler, U. Raut, M. Famá and R. A. Baragiola, Astrophysical Journal Letters, 2006, **644**, L141–L144.
11 C. P. Ennis, C. J. Bennett and R. I. Kaiser, Physical Chemistry Chemical Physics (Incorporating Faraday Transactions), 2011, **13**, 9469.
12 C. J. Bennett and R. I. Kaiser, Astrophysical Journal, 2005, **635**, 1362–1369.
13 B. Sivaraman, C. S. Jamieson, N. J. Mason and R. I. Kaiser, Astrophysical Journal, 2007, **669**, 1414–1421.
14 B. Sivaraman, A. M. Mebel, N. J. Mason, D. Babikov and R. I. Kaiser, Physical Chemistry Chemical Physics (Incorporating Faraday Transactions), 2011, **13**, 421.
15 C. Janssen, Journal of Geophysical Research (Atmospheres), 2005, **110**, D08308.
16 D. Jing, J. He, J. R. Brucato, G. Vidali, L. Tozzetti and A. De Sio, Astrophysical Journal, 2012, **756**, 98.
17 D. Jing, J. He, J. R. Brucato, G. Vidali, L. Tozzetti and A. De Sio, Astrophysical Journal, 2014, **780**, 113.
18 M. Jonusas and L. Krim, Monthly Notices Royal Astronomical Society, 2016, **459**, 1977–1984.
19 D. Fulvio, B. Sivaraman, G. A. Baratta, M. E. Palumbo and N. J. Mason, Spectrochimica Acta Part A: Molecular Spectroscopy, 2009, **72**, 1007–1013.
20 C. J. Bennett, C. Jamieson, A. M. Mebel and R. I. Kaiser, Physical Chemistry Chemical Physics (Incorporating Faraday Transactions), 2004, **6**, 735.
21 K. Yanallah, F. Pontiga and A. Castellanos, Journal of Physics D Applied Physics, 2011, **44**, 055201.
22 H. Chaabouni, L. Schriver-Mazzuoli and A. Schriver, Journal of Low Temperature Physics, 2000, **26**, 712–718.
23 M. A. Ovchinnikov and C. A. Wight, Journal of Chemical Physics, 1995, **102**, 67–74.
24 H. Chaabouni, L. Schriver-Mazzuoli and A. Schriver, Journal of Physical Chemistry A, 2000, **104**, 6962–6969.
25 R. Siebert, P. Fleurat-Lessard, R. Schinke, M. Bittererová and S. C. Farantos, Journal of Chemical Physics, 2002, **116**, 9749–9767.

26 D. H. Parker, Accounts of Chemical Research, 2000, **33**, 563–571.
27 M. A. A. Clyne, B. A. Thrush and R. P. Wayne, Photochemistry and Photobiology, 1965, **6**, 957.
28 H. Akimoto and J. Pitts, Journal of Chemical Physics, 1970, **53**, 1312–1315.
29 A. Bar-Nun, G. Herman, M. L. Rappaport and Y. Mekler, Surface Science, 1985, **150**, 143–156.
30 C. Janssen, J. Guenther, D. Krankowsky and K. Mauersberger, Journal of Chemical Physics, 1999, **111**, 7179–7182.
31 J. Morton, J. Barnes, B. Schueler and K. Mauersberger, Journal of Geophysical Research, 1990, **95**, 901–907.

This journal is © The Royal Society of Chemistry [year]